Improved electronic structure prediction of chalcopyrite semiconductors from a semilocal density functional based on Pauli kinetic energy enhancement factor

Arghya Ghosh,[1,*] Subrata Jana,[2,†] Manish K Niranjan,[1,‡] Sushant Kumar Behera,[2] Lucian A. Constantin,[3] and Prasanjit Samal[2]

[1] *Department of Physics, Indian Institute of Technology, Hyderabad, India*
[2] *School of Physical Sciences, National Institute of Science Education and Research, HBNI, Bhubaneswar 752050, India*
[3] *Istituto di Nanoscienze, Consiglio Nazionale delle Ricerche CNR-NANO, 41125 Modena, Italy*

(Dated: May 25, 2021)

The correct treatment of d electrons is of prime importance in order to predict the electronic properties of the prototype chalcopyrite semiconductors. The effect of d states is linked with the anion displacement parameter u, which in turn influences the bandgap of these systems. Semilocal exchange-correlation functionals which yield good structural properties of semiconductors and insulators often fail to predict reasonable u because of the underestimation of the bandgaps arising from the strong interplay between d electrons. In the present study, we show that the meta-generalized gradient approximation (meta-GGA) obtained from the cuspless hydrogen density (MGGAC) [Phys. Rev. B 100, 155140 (2019)] performs in an improved manner in apprehending the key features of the electronic properties of chalcopyrites, and its bandgaps are comparative to that obtained using state-of-art hybrid methods. Moreover, the present assessment also shows the importance of the Pauli kinetic energy enhancement factor, $\alpha = (\tau - \tau^W)/\tau^{unif}$ in describing the d electrons in chalcopyrites. The present study strongly suggests that the MGGAC functional within semilocal approximations can be a better and preferred choice to study the chalcopyrites and other solid-state systems due to its superior performance and significantly low computational cost.

I. INTRODUCTION

In the last two decades, the ABX_2 (A=Cu,Ag,Be,Cd,Mg,Zn; B=Ga,Ge,In; X=S/Se/Te) chalcopyrite semiconductors based on the zinc-blend structure have emerged as highly promising advanced solar cells materials that allow the tweaking of macroscopic physical properties as function of microscopic chemical and structural degrees of freedoms[1–6]. In particular, Cu-based ternary and quaternary semiconductors and their alloys are now widely exploited as light absorbers in thin film solar cells[2,7–10] and various non liner optical devices[11–13]. Unfortunately, the theoretical predictions of the structural and electronic properties of Cu-based multinary semiconductors remain far from being accurate because of the involvement of semicore d or f electrons, which play a decisive role in the determination of the properties of these materials[14,15].

The straightforward applications of the Kohn-Sham (KS) density functional theory (DFT)[16] within the framework of the local density approximation (LDA)[17] or generalized gradient approximation (GGA)[18] often result in wrong predictions of bandgaps and band ordering as these suffer from the delocalization error[19]. Thus, the insufficiency and lack of appropriate theoretical approaches hinder the proper understanding of the inherent electronic properties of these systems. Although, some plausible attempts have been made to correlate bandgap with the physical parameters in chalcopyrites such as $CuInSe_2$, $CuInS_2$ in various literature[14,20], theoretical studies of such correlations and structural anomalies in relevant and important prototypes such as $CuGaS_2$, $CuAlS_2$, are still fragmentary.

Nevertheless, using hybrid functional schemes[21–28], improved bandgaps of chalcopyrites and other insulators have been reported. These schemes combine Hartree-Fock exchange with LDA/GGA correlation. Further, the semilocal exchange-correlation (XC) effect of strongly localized d-orbitals are treated at the mean-field level[29–32]. Although the hybrid density functionals have been applied and studied for a variety of systems, these schemes are often computationally expensive and prohibitive. On the other hand, the strong electron correlations and self-interaction related problems within semilocal approximation can be partially mitigated by the addition of separate Hubbard U for the d or/and f localized electrons. This scheme may be expected to provide a qualitative assessment of the influence of the electronic correlations on the physical properties of a system[29,30]. The DFT+U method attempts to fix hybridization problems due to overly-delocalized orbitals and thereby has been recognized as a potent tactic to treat the strongly localized d electrons in chalcopyrites[31,32].

In addition to hybrid and DFT+U schemes, the quasiparticle correction method within the many-body GW approximation is even more well-founded among different levels of theory which renders a relatively more accurate estimation of bandgaps[29,30]. However, the calculations using the GW scheme are usually more computationally expensive than those using hybrid functionals.

Over the years, the search for efficient semilocal approaches which can predict the accurate electronic structure of systems, has become an important and fascinating research topic. The progress in semilocal density functionals in recent years shows that the accuracy of the material properties can be achieved from the advanced XC methods by satisfying more exact quantum mechanical constraints. The advent of these accurate semilocal

density functionals[33–38] has also led to wide applicability of DFT in the condensed matter physics. In particular, the meta-GGA functionals have been found to be quite successful in overcoming the several challenges associated with the lower rung of functionals such as GGA, LDA etc.[39–45]

Though the chalcopyrite systems have been studied using different functionals, the assessment, and performance of the advanced meta-GGA methods for these systems have not been reported to the best of our knowledge. Therefore, in this article, we investigate the performance of some advanced meta-GGA functionals such as 1) meta-GGA functional obtained from the cuspless hydrogen density (MGGAC)[35], 2) strongly constrained and appropriately normed (SCAN) semilocal functional[33] , and 3) Tao-Mo (TM)[34] semilocal functional. We assess the performance of these functionals in the study of structural and electronic properties, bandgaps, and enthalpy formation energies of chalcopyrite systems. It may be noted that both SCAN and MGGAC functionals have been found to be quite successful in overcoming the several drawbacks of the GGA functional such as severe underestimation of the bandgaps of the bulk and layered solids[46]. In particular, our study shows that the MGGAC functional is quite advantageous to study the chalcopyrite semiconductors as it is computationally inexpensive and exhibits good performance. The aforementioned meta-GGA schemes span the third rung of the Jacob ladder of the XC approximation[47] owing to important features associated with them.

This paper is organized as follows. The methodologies used in this work are discussed in section II. The structural properties, electronic properties, and enthalpy formation energies are discussed in sections II, III, and IV respectively. The results and the functional performances are further analyzed in section VI. Finally, the conclusions are presented in section VI.

II. COMPUTATIONAL METHODS

The density functional calculations are performed using the plane-wave formalism as implemented in Vienna Ab-initio Simulation Package (VASP) code[48–51]. The core-valence electron interaction is approximated using the projected augmented wave (PAW) method[52]. A kinetic energy cutoff of 600 eV is used to expand the Kohn-Sham (KS) single-particle orbitals on a plane-wave basis. The Brillouin Zones (BZ) are sampled using Monkhorst-Pack $9 \times 9 \times 9$ **k**-points grid for atomic relaxations and 17×17×17 grid for the density of states (DOS) calculations. The electronic energies are allowed to converge up to 10^{-6} eV (or less) to achieve self-consistency in the calculations. The atomic relaxations are performed till the Hellmann-Feynman forces on atoms are reduced to less than 0.01 eV/Å.

The exchange-correlation (XC) contributions are included using semilocal XC functional schemes such as PBE[18], SCAN[33], MGGAC[35], and TM[34]. Unlike GGAs, the meta-GGA functionals SCAN, MGGAC, and TM are implemented in generalized KS (gKS)[53,54] scheme because of their dependence on KS orbitals. Usually, the meta-GGAs are quite reliable as compared to GGAs as they can recognize and describe covalent, metallic, and non-covalent interactions [55,56].

TABLE I. I-III-VI2 and I-IV-V2 chalcopyrite semiconductor systems considered in this paper.

Group	Systems
I-III-VI2	$CuInS_2$, $CuInSe_2$, $CuGaS_2$, $CuGaSe_2$, $CuAlS_2$, $CuAlSe_2$, $CuAlTe_2$, $CuGaTe_2$, $CuInTe_2$, $AgAlS_2$, $AgAlSe_2$, $AgAlTe_2$, $AgGaS_2$, $AgGaSe_2$, $AgGaTe_2$, $AgInS_2$, $AgInSe_2$, $AgInTe_2$
II-IV-V2	$BeSiP_2$, $BeSiAs_2$, $BeGeP_2$, $BeGeAs_2$, $BeSnP_2$, $BeSnAs_2$ $MgSiP_2$, $MgSiAs_2$, $MgGeP_2$, $MgGeAs_2$, $MgSnP_2$, $MgSnAs_2$ $ZnSiP_2$, $ZnSiAs_2$, $ZnGeP_2$, $ZnGeAs_2$, $ZnSnP_2$, $ZnSnAs_2$ $CdSiP_2$, $CdSiAs_2$, $CdGeP_2$, $CdGeAs_2$, $CdSnP_2$, $CdSnAs_2$

In general, the meta-GGA XC functional which depends on the density (ρ), gradient of density ($\nabla\rho$), and KS kinetic energy density ($\tau(\mathbf{r}) = \frac{1}{2}\sum_i |\nabla\psi_i|^2$) can be presented as:

$$E_{xc}[\rho_\uparrow, \rho_\downarrow] = \int d^3r\, \rho(\mathbf{r}) \epsilon_x^{LDA} F_{xc}(\rho_\uparrow, \rho_\downarrow, \nabla\rho_\uparrow, \nabla\rho_\downarrow, \tau_\uparrow, \tau_\downarrow)\,, \tag{1}$$

where ϵ_x^{LDA} is the exchange energy density in uniform electron gas approximation and F_{xc} is the XC enhancement factor. In case of construction of SCAN[33] and MGGAC[35] functionals, one of the main ingredients in F_x is the Pauli kinetic enhancement factor $\alpha = (\tau - \tau^W)/\tau^{unif}$, where $\tau^W = |\nabla\rho|/[8\rho]$ is the von Weizsäcker kinetic energy density, $\tau^{unif} = 3/10(3\pi^2)^{2/3}\rho^{5/3}$ is the Thomas-Fermi kinetic energy density, and $k_F = (3\pi^2\rho)^{1/3}$ is the Fermi wave vector. It may be noted that the exchange of the SCAN functional uses both the α and $p = s^2$, while the exchange in MGGAC uses only α. This makes MGGAC F_{xc} in exchange-only or high-density limit ($r_s \to 0$) independent of s. Importantly, both SCAN and MGGAC respect the tightened bound of the exchange ($F_x \leq 1.174$[33,57]) and possess negative slope with respect to α ($\partial F_x/\partial\alpha < 0$), important for the bandgap improvement in semilocal level[35,46,58].

Another reliable meta-GGA semilocal functional was proposed by Tao-Mo (TM)[34] which has been quite successful at providing reasonably accurate estimates of various quantum chemical and solid-state properties[34,39,59–61]. The TM and its revised version revTM[39] functionals, use both the meta-GGA ingredients i.e., $z = \tau^W/\tau$ and α. However, these functionals satisfy looser bound of exchange[62–64] and suffer from the order-of-limit problem[37].

In addition to aforementioned functionals, we have also used the hybrid functional HSE06 scheme propounded by Hyde, Scuseria, and Ernzerhof[21–24]. The HSE06 scheme is based on the inclusion of fixed amount of Hartree-Fock exchange. Briefly, the exchange-correlation energy of the HSE06 functional is given by[21–24],

$$E_{xc}^{HSE}(\alpha,\omega) = \alpha E_x^{HF,SR}(\omega) + (1-\alpha) E_x^{PBE,SR}(\omega) + E_x^{PBE,LR}(\omega) + E_c^{PBE} \ . \quad (2)$$

Here, the exchange-correlation energy E_{xc} is range separated with the use of a screening potential. The parameter α describes the fraction of the Fock exchange while ω calibrates the range of the interaction. We have used the conventional $\alpha = 0.25$ and $\omega = 0.11$ bohr^{-1} in computations with HSE06[23,24]. It may be noted that other variants of hybrid density funtionals[25–28] have also been proposed.

In this work, we report the relative performance of HSE06, MGGAC, PBE, SCAN, and TM functionals by comparing the computed estimates of the structural parameters and properties of the Cu based chalcopyrite systems. In case of other systems, the structural properties are calculated only using MGGAC, PBE, SCAN, and TM functionals and the results are reported in supplementary material[65]. Since, the main focus of the present work is the study of Cu based chalcopyrites, we do not relax the structures of Ag, Be, Cd, Mg, and Zn based chalcopyrites using HSE06 scheme, which is quite expensive computationally. For these systems the structures are optimized and lattice constants are computed using PBE (GGA) scheme.

In Table I, we list the I-III-VI2 and II-IV-V2 group systems which are considered in present work.

III. STRUCTURAL PROPERTIES

The chalcopyrite lattice structure adopts the D_{2d}^{12} (No.122) space group symmetry. The structure is a cation mutated super-structure of the cubic zinc-blende structure (T_d^2), in which each of the two cations (A, B) are tetrahedraly coordinated by four anions (X), and each anion is coordinated by two A and two type B cations[66]. The chalcopyrite structure can be described accurately by three structural parameters: (i) lattice constant a, (ii) the tetragonal ratio $\eta = c/2a \neq 1$, where c is the lattice constant in the z-direction, and (iii) the anion displacement parameter, u. In general, $A-X$ and $B-X$ bond lengths, denoted by r_{A-X} and r_{B-X}, respectively, are not equal. This unequal anion-cation bond length results in a tetragonal distortion vis-a-vis an ideal zinc blende structure. The distortion parameter $u = 0.25 + (r_{A-X}^2 - r_{B-X}^2)/a^2$, which describes the repositioning of the anions in the $x-y$ plane, sensitively influence the bulk electronic bandgap of these materials[66].

The ternary ABC_2 [A = I; II = Cu, Ag; Be, Mg, Zn, Cd, B = III; IV = In, Ga, Al; Si, Ge, Sn, and C = VI; V = S, Se, Te; P, As] chalcopyrite compounds of composition I−III−VI_2 or II−IV−V_2 are iso-electronic analogous of the II−VI or III−V binary semiconductors, respectively[67]. The crystal structure of these chalcopyrites is described by D_{2d}^{12} ($I42d$) space group symmetry, and can be regarded as a super-lattice of the zinc-blende structure with small structural distortions[4]. The lattice constants (a and c), distortion parameter (u), and tetragonal ratio (η) of Cu based chalcopyrites computed using different XC schemes are listed in Table S1 of the supporting information[65]. The trend seen in the results obtained from semilocal functionals may be explained from the perspective of computed electronic properties.

In general, the computed lattice constants of solids obtained from PBE-like GGA XC functionals are reasonably accurate. However, the PBE-GGA computed lattice constants are generally found slightly overestimated because of the lack of slowly varying density correction, which is taken care of in its solid-state version PBEsol[68,69]. Furthermore, the higher rung of functionals i.e., meta-GGAs are generally better than PBE-GGA functional for estimating the lattice constants. For instance, the SCAN meta-GGA performs reasonablly well in predicting the lattice constants of different solids.

In Fig 1, we show the relative error (in %) in parameters a, c, u, and η of the Cu based chalcopyrites as obtained from different methods. As can be seen, the HSE06 performs better than other methods. However, within semilocal methods, the SCAN performs better than MGGAC and PBE for a and c, while MGGAC performs better than SCAN for u. Further, in most cases, the MGGAC underestimates a and c parameters as compared to experimental and SCAN values. It may also be noted that for the tetragonal ratio (η), the MGGAC performs in a more balanced way than SCAN due to its tendency to underestimate both a and c. Physically, the improvements in u obtained using MGGAC as compared to those obtained using SCAN comes from bond lengths $r_{A/B-X}$, which are also significantly improved by much better description of the Cu d-states. It may also be seen in Fig 1 that the u parameters obtained from MGGAC are very close to those obtained using HSE06. This indicates that the performance of MGGAC is quite close to that of HSE06 in treating Cu-d states. We will further discuss this point in more detail in section IV.

IV. ELECTRONIC PROPERTIES

The phenomenological treatment of p-d interaction in chalcopyrite systems depends on how good are the various approximation of XC for the d-electron of Cu. For instance, the LDA (or GGA) based methods tend to delocalize d-electrons which results in underestimation of $p-d$ hybridization [14,32].

Further, a significant shortcoming in standard DFT based methods is the presence of inherent self-interaction error (SIE)[14,70]. In the case of chalcopyrites, this shortcoming results in shallow d states description for the cations, and in general, the absence of derivative discontinuity in the KS bandgap which is defined as the difference between eigenvalues of the CBM and VBM. As a consequence, the theoretical bandgap is severely un-

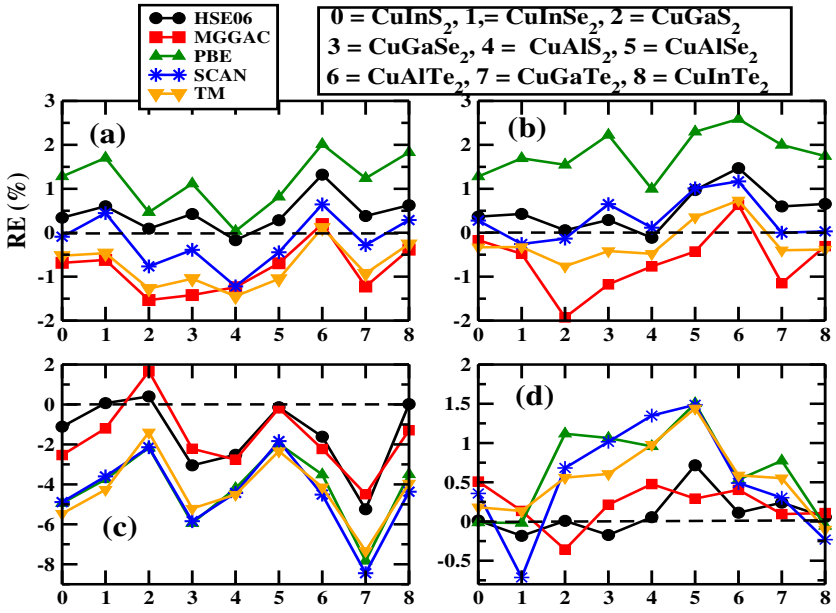

FIG. 1. Relative error (%) in (a) in-plane lattice constants, (b) lattice constants in z direction, (c) distortion parameter (u), and (d) tetragonal ratio (η) of the Cu based chalcopyrite systems reported in Table S1 of the supporting information[65]. The levels along $x-$ axis is same as the solids presented in Table S1 of the supporting information[65] and shown in the caption.

derestimated as compared to the experimental bandgap (the difference between the ionization potential and electron affinity). The absence of the LDA/GGA computed bandgaps in some of the chalcopyrites and other material systems has been attributed to large ratio of SIE in exchange functionals. Hybrid functionals eliminate some amount of SIE and improve the performance and estimates of bandgaps[14,70]. The performance of the meta-GGA functionals which are implemented in gKS scheme (such as SCAN and MGGAC), in providing estimates of the electronic properties of chalcopyrites has not been reported. We discuss these in next subsection.

To evaluate the relative performances of different functionals, we first discuss the band structures as obtained from HSE06, MGGAC, PBE, and SCAN functionals. Following this, the density of states (DOS) and charge density will be analyzed and discussed. We have not included the performance of the TM functional here as its performance is known to lie in between that of PBE and SCAN functionals. The bandgap values computed using TM functional are shown in Table S1 of the supporting information[65]. Overall, the performance of TM functional is found to qualitatively similar to that of the PBE functional.

In order to analyze the performance of different functionals, the band structures, charge density, and DOS of $CuInS_2$ are computed using the HSE06, MGGAC, PBE, and SCAN functionals. In supporting information[65], we also present and analyze the electronic properties of $CuInSe_2$. These two systems are particularly chosen since their electronic band structures, density of states (DOS), and charge densities are quite distinct from one another. Further, both these systems are known to exhibit strong interplay between structure and electronic properties[14].

A. Band structures

The bandgaps of different Cu-based chalcopyrite systems as obtained from different methods are shown in Table S1 of the supporting information[65]. As can be seen, the bandgaps computed using hybrid HSE06 method, are in close agreement with the experimental values. Further, among the semilocal functionals, MGGAC performs in a significantly better way than others, as it opens the bandgaps in $CuInS_2$, $CuInSe_2$, and $CuInTe_2$. The bandgaps computed using SCAN, TM and PBE are found to be severely underestimated and thus these methods perform poorly.

Fig 2 shows the band structure of $CuInS_2$ along high-symmetry directions in BZ. As can be seen, the bandgap computed using MGGAC is improved significantly and is quite close to that obtained using HSE06. The SCAN method though opens the bandgap for $CuInS_2$, its magnitude comes out to be very small. The use of PBE results in zero bandgap.

It may be noted that the HSE06 functional has more often been used to study chalcopyrites as compared to other global hybrid functionals such as PBE0, because of the presence of screened Coulomb interaction, which reduces the computational cost significantly.

As can be seen in Table S1 of the supporting information[65], excellent estimates of electronic properties are obtained from hybrid functional HSE06 with its default value of 25% fraction of Fock exchange.

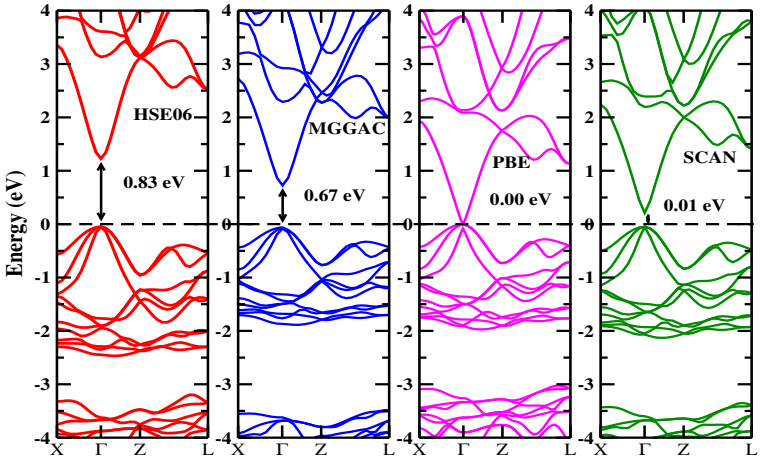

FIG. 2. Band structures of $CuInS_2$ as obtained from different methods.

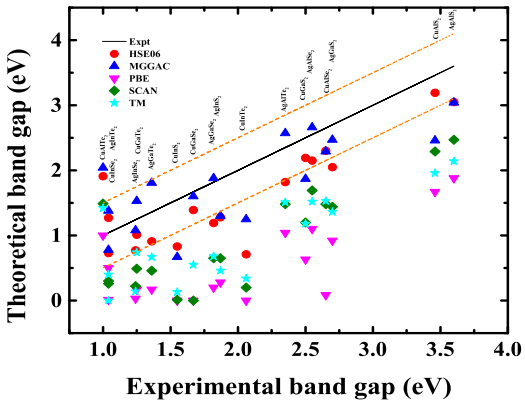

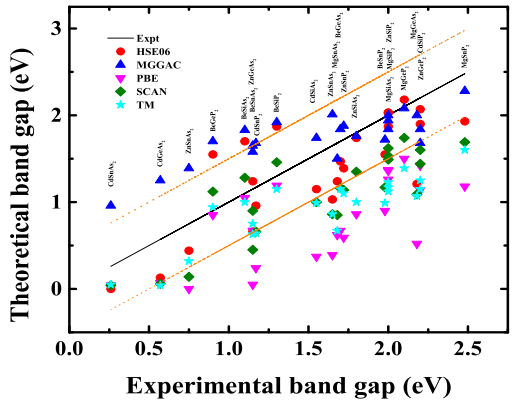

FIG. 3. Experimental versus theoretical bandgaps of I-III-VI2 (upper panel) and II-IV-V2 (lower panel) semiconductors as obtained from different methods. The values within dotted lines indicate the bandgaps within the error of ±0.5 eV of the experimental values. The experimental bandgaps of I-III-VI2 are taken from ref.[71] and II-IV-V2 from ref.[67].

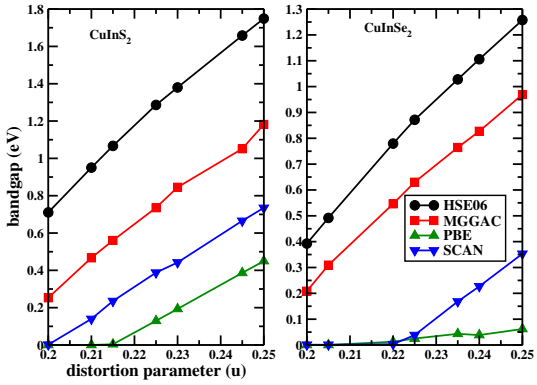

FIG. 4. Variation of bandgaps of $CuInS_2$ and $CuInSe_2$ as a function of distortion parameter (u).

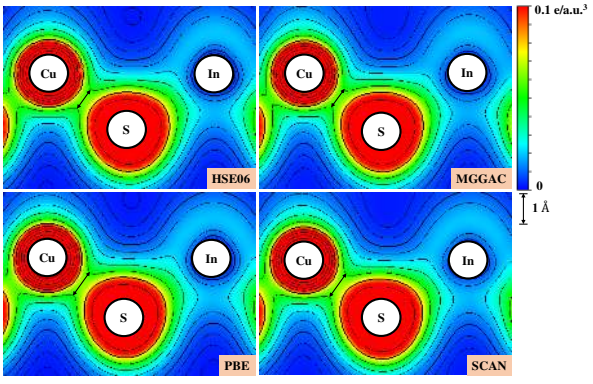

FIG. 5. Electronic charge density distribution contours of $CuInS_2$ in the plane contain the Cu, In, and S atoms according to different methods. The logarithmic scale is used for the clear visualization of the isosurfaces.

Interestingly, among considered semilocal approximations, the MGGAC functional performs quite closely to HSE06 for most semiconductors. (see supplemental material). A comparative plot of theoretical and experimen-

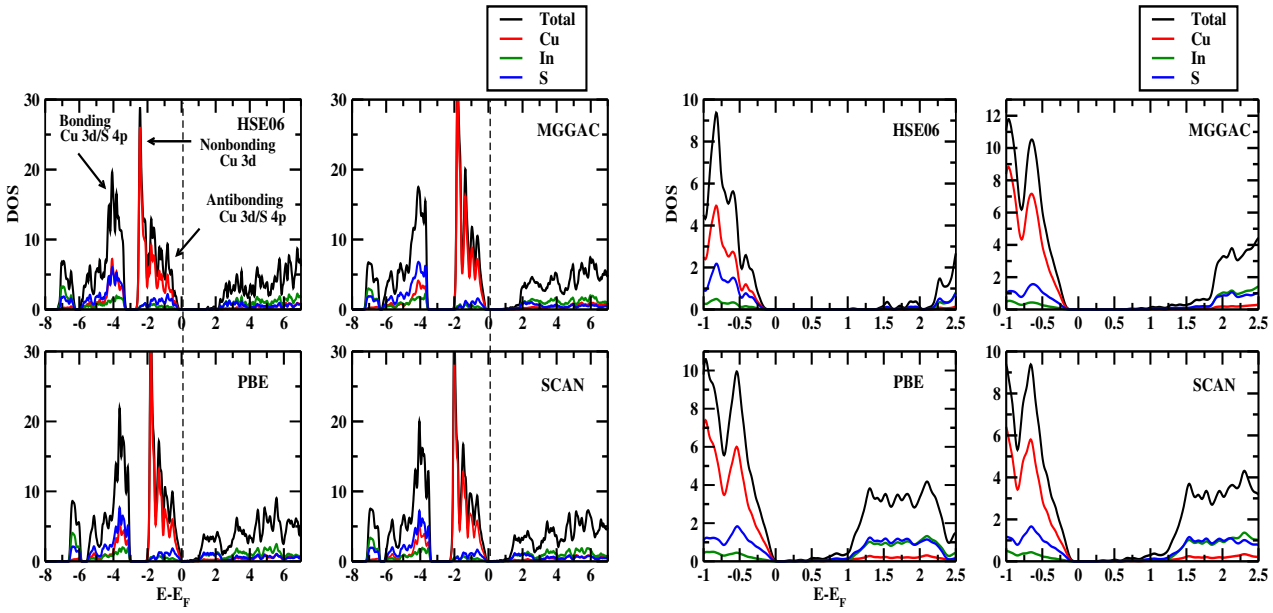

FIG. 6. Density of states (DOS) for $CuInS_2$ calculated from different methods. Right panel shows the DOS in energy range $-1\ eV < (E - E_F) < 2.5\ eV$. The Fermi energy ($E_F$) is set to 0 eV and is same as E_{VBM}.

tal bandgaps is shown in Fig 3 which clearly indicates that bandgap estimates obtained using MGGAC are more accurate than those obtained using other semilocal functionals.

Based on the comparision of the results presented in this work with those in Ref.[67,72] for I-III-VI2 and II-IV-V2 chalcopyrite semiconductors, the performances of different functionals are twofold:

- **I-III-VI_2 semiconductors:** The direct bandgaps are found to be most severely underestimated when computed using semilocal functionals like GGA, SCAN, and TM. For Ag based chalcopyrites too, a similar trend is observed. A consistent improvement in the bandgap magnitudes is observed, when computed using the MGGAC functional. This is expected due to the improvement in the description of $p - d$ hybridization discussed in the previous section. In the case of $CuAlTe_2$, the bandgap computed using MGGAC and HSE06 is found to be overestimated whereas PBE-GGA estimate of the bandgap is closer to the experiment. Further, for all the Te based systems, MGGAC overestimates the bandgaps as compared to HSE06. In particular, the MGGAC overestimates the bandgaps of $CuAlTe_2$ and $AgInTe_2$ by a large margin. Nevertheless, for other Te based systems, the performance of MGGAC is reasonably good with bandgap estimates closer to the experiments as compared to other semilocal methods.

- **II-IV-V2 semiconductors:** The computed GGA bandgaps are found to be in excellent agreement with the experiments[67] and earlier reported theoretical results[67]. The MGGAC computed bandgaps are found to be comparable with HSE06 computed bandgaps. However, both MGGAC and HSE06 overestimate the bandgaps in case of $BeSiAs_2$, $BeSiP_2$, $CdGeAs_2$, $CdSnP_2$. In case of these semiconductors, the SCAN functional performs well as compared to other semilocal (MGGAC, TM, GGA) methods (see ref.[65] for details). As can be seen in Fig 3, the MGGAC computed bandgaps are overestimated by more than 0.5 eV in case of $CdSnAs_2$, $CdGeAs_2$, $ZnSnAs_2$, $BeGeP_2$, $BeSiAs_2$, and $BeSiP_2$.

It may be noted that for chalcopyrite semiconductors containing Be and Cd, the HSE06 bandgaps are comparable to the GW_0 bandgaps as reported in Ref.[67]. Further, the semilocal functionals SCAN, TM, GGA underestimate the bandgaps. However, MGGAC overestimates the bandgap for $BeSiAs_2$, $BeSiP_2$, $CdGeAs_2$, $CdSnP_2$. In case of $BeGeAs_2$ and $BeSnP_2$, MGGAC bandgaps are comparable to the experimental values and are in better agreement than that for HSE06 functional.

For semiconductors containing Mg and Zn, all functionals estimate bandgaps close to the experimental values except for some semiconductors containing Zn.

Overall, it may be concluded from the calculations and above discussions that the bandgaps estimated by semilocal MGGAC are comparable to those estimated by hybrid functional HSE06 to a great extent with a minimal deviation (see Fig 3).

To visualize the variation of the bandgap with the distortion parameter (u), we plot in Fig. 4 the bandgaps of $CuInS_2$ and $CuInSe_2$ computed using different functionals as a function of u. As can be seen, the bandgap increases almost linearly with u in range $0.2 < u < 0.25$.

For both the chalcopyrite systems, HSE06 bandgaps are improved over MGGAC bandgaps, which in turn are improved over SCAN bandgaps. For $CuInS_2$ and $CuInSe_2$, the SCAN bandgap opens for $u > 0.2$ and $u > 0.22$, respectively. As can be seen, the MGGAC and HSE06 bandgaps are finite for all values of u (in range shown) for both the chalcopyrites. The difference in the bandgaps obtained from different methods is expected due to strong interplay between the structure parameter u and the hybridization of the $p-d$ orbitals[14]. We will revisit this point later in this paper.

In supporting information[65], we also discuss and analysis another chalcopyrite system $CuInSe_2$. As can be seen in supporting information[65], the MGGAC and HSE06 open the bandgap of this system, whereas it remains closed for PBE and SCAN functionals.

B. Charge densities

The charge density contours for $CuInS_2$ are shown in Fig.5, which reveals the the presence of both ionic and covalent bonds. The mixed bonding is seen irrespective of the XC functionals used. As can be seen, the electron density is more enhanced towards the side of the S-atom than that of the In-atom, which indicates that the In−S bond is more ionic. Further, the even distribution of the electron density in the case of the Cu−S bond indicates that the bonding is more covalent. The arrow labeled in the Cu−S bond (see Fig. 5) indicates the isosurface value. The size of the arrow is larger in the case of PBE and SCAN than the one for MGGAC and HSE06, which follows the bandgap enlargement rule as well as the differences in the u parameter as the arrow size is related to the corresponding bond length and varying degrees of $p-d$ hybridization for these chalcopyrites. From Table S1 of the supporting information[65], it can be seen that the calculated u parameter, which depends on the bond length of Cu−S, is less for PBE and SCAN (0.218) than that for MGGAC (0.224) and HSE (0.226). The greater the isosurface arrow, the lower the atomic distance is, which indicates greater $p-d$ repulsion and thereby smaller bandgap. It is generally understood that methods (within the DFT framework) that do not take into account the self-energy correction, underestimate the bandgaps. However, in the case of MGGAC, the presence of internal screened coulomb energy U results in bandgap estimates which are comparable to bandgaps obtained using hybrid functionals as well as state-of-the-art many-body perturbation technique. We will revisit and elaborate more on this point in a later section. The MGGAC computed bandgaps also exhibit general trend which is similar to that seen for bandgaps obtained using other functionals. For instance, the computed bandgaps of semiconductors containing P-atoms are always larger than bandgaps of semiconductors containing As-atoms.

C. Density of states

The electronic structures of all chalcopyrite semiconductors are qualitatively similar. In the following, we present and discuss the electronic structure of $CuInS_2$. The electronic structure of $CuInSe_2$ is presented in the supporting information[65]. The total density of states (DOS) and partial DOS as computed with different XC functionals are shown in Fig 6 and Fig. S3 of supporting information[65] for $CuInS_2$ and $CuInSe_2$, respectively. As can be seen, the contribution from the valence Cu-4s and Cu-3p states near the VBM is negligible as compared to Cu-3d states. The valence band region exhibits two main groups: up to around −2 eV from the VBM, the region is mainly composed of p and d states with primary contribution from Cu−3d states. The deeper valence band in the energy range -2 eV to 0 eV results from strong hybridization of Cu−3d and S−3p states. The conduction band region is contributed by In−5p and S−3p states along with a minor contribution of Cu−3d states. The dispersion of the valence and conduction bands are found to be almost the same for all semilocal functionals (GGA, SCAN, and MGGAC) with an exception that the band width (energy between the highest and lowest allowed levels) for MGGAC is wider than that for PBE and SCAN.

To encapsulate the behavior of the VBM and CBM, we show the DOS plot for the respective functionals in the right panel of Fig 6, in the energy range $-1\ eV < (E - E_F) < 2.5\ eV$. The enhancement in the bandwidth is evident in case of MGGAC as compared to that for SCAN and PBE semilocal functionals. In case of MGGAC, the CBM shifts to the higher energy level due to slightly enhanced hybridization between Cu−3d and S−3p states at VBM, resulting in the opening of the bandgap. However, in case of PBE and SCAN, the 3d non-bonding region lies a little bit of the higher side on the energy scale, which results in the reduction of the bandgap as compared to that in case of MGGAC and HSE06.

In the case of HSE06, the relative bandgap enhancement compared to that for semilocal functionals happens because of the inclusion of the non-local HF exchange, which reduces the repulsion between Cu−3d and S−4p states and thereby results in the bandgap opening[70]. Importantly, the bandgap enlargement in the case of HSE06 as compared to other semilocal functionals (MGGAC, SCAN, TM, and PBE) may be attributed to (i) enlargement of bandwidth and the orbital spacing which directly influences the bandgap and (ii) the shift of non-bonding 3d states downward which reduce the $p-d$ repulsion.

Nevertheless, the performance of the MGGAC within semilocal XC functionals is quite encouraging and the same trend of results also follows for all I-III-VI2 semiconductors as the valence band maximum is influenced by the 4d states of I-group atoms. On the other hand, in the case of II-IV-V2 semiconductors, the bandgap character is not influenced by d states of II-group atoms, as these are highly localized and contribute to valence bands

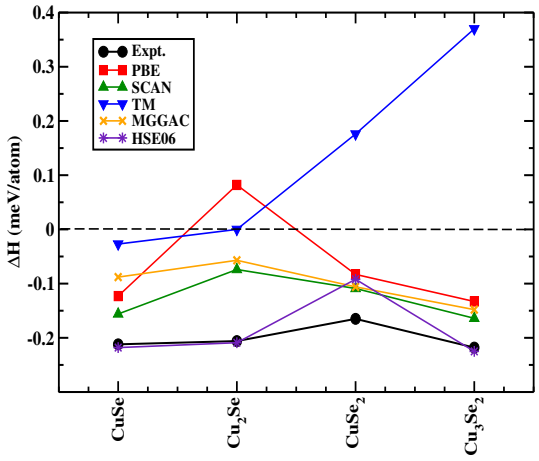

FIG. 7. Enthalpy formation energies (meV/atom) of Cu-Se binaries as obtained from different methods

far from VBM[67].

In supporting information[65], we show the DOS and PDOS for $CuInSe_2$. In this case also, the opening of the bandgap can be explained sililarly as discussed for $CuInS_2$. The reduction in repulsion between Cu$-3d$ and Se$-4p$ states is responsible for the opening of bandgap. For MGGAC, this repulsion reduces at the VBM and the CBM is shifted towards the higher energy. This results in the opening of the bandgap more than that in case of SCAN.

V. FORMATION ENTHALPIES

We now discuss the enthalpy formation energies of chalcopyrites and competing binary phases of Cu-Se, computed using different meta-GGA functionals. In the thermodynamical framework, the enthalpy formalism energy per atom for a chalcopyrite system is defined as:

$$\Delta H = [\epsilon_{system} - \sum_i n_i \epsilon_i]/m \ , \qquad (3)$$

where ϵ_{system} is the energy of the chalcopyrite system, n_i and ϵ_i are the number and energy of the i^{th} constituent in the system, and m is the total number of atoms in the system. All energies are calculated in their stable solid form. A negative (positive) enthalpy formation energy indicates that the system is stable (unstable).

The Table II shows the formation enthalpies of $CuInSe_2$ and $AgInSe_2$ computed using different functionals. For these solids, the experimental formation enthalpies have been reported in ref.[73]. The PBE and HSE06 results in Table II are taken from ref.[70]. As can be seen, the PBE underestimates the formation energies of both the chalcopyrites by more than 30%. The SCAN method improves the enthalpy estimates as compared to those obtained using PBE. The SCAN values are underestimated by less than 30%. Further, Table II shows that the formation enthalpy estimates are improved significantly with the use of MGGAC functional, which performs as accurately as hybrid HSE06 functional and with computational cost much lesser than that of HSE06.

It may be noted that the PBE functional does not properly describe different bondings such as metallic, covalent, and/or ionic in different solids[74–76]. The bonding nature is much better described by meta-GGA[55] functionals, which is reflected in the performance of SCAN and MGGAC. This is because the meta-GGA functionals are generally better than GGAs in describing the covalent, metallic, and non-covalent interactions [55,56].

Incidentally, the TM functional fails drastically in providing reasonable estimates of formation energies as it exhibits error more than PBE. This failure of the TM may be attributed to its order-of-limit problems, which is important for estimating the formation of enthalpies[37]. In case of the HSE06, the good performance is due to reasonably correct desprition of the d-states of Cu and Ag atoms.

The formation enthalpy of $CuInSe_2$ computed using MGGAC and HSE06 is in close agreement with the experiments, which is expected due to improved estimates of energy eigenvalues, In-4d states, band structure and DOS in it (see supporting material[65]).

Next, we assess the functionals performance for the several competing candidate binary phases of Cu-Se. The formation enthalpies per atom for different Cu$-$Se phases are plotted in Fig. 7. As expected, PBE underbinds the formation enthalpies, with a positive ΔH for Cu_2Se compound. The HSE06 estimated formation energies are found to be in closest agreement with the experimental values. The SCAN and MGGAC perform closely, albeit SCAN performance slightly better than MGGAC in all cases. This may be partially attributed to the metallic character of the CuSe, $CuSe_2$, and Cu_3Se_2, which is better described by the SCAN functional as it takes into account the slowly varying second/fourth order terms in the gradient expansion of the exchange. Furthermore, the SCAN correlation is free from spurious one-electron self-interaction which tends to improve the formation enthalpy estimates. Nevertheless, both SCAN and MGGAC formation energies are negative (including semiconductor Cu_2Se) and therefore are much better estimated as compared to those by PBE-GGA. Fig. 7 also shows that the performance of the TM functional is quite poor for all the binary phases of Cu-Se. As can be seen, the TM functional incorrectly predicts $CuSe_2$ and Cu_3Se_2 as unstable. This significantly poor performance of the TM functional in providing formation enthalpy estimates may be attributed to its order-of-limit problem[37].

TABLE II. Enthalpy formation energies (eV/f.u.) of $CuInSe_2$ and $AgInSe_2$ as obtained from different methods. PBE and HSE06 values are taken from ref.[70]. Numbers in the parentheses represent the percentage deviation.

Solids	PBE	SCAN	TM	MGGAC	HSE06	Expt.[73]
$CuInSe_2$	-1.78	-2.02	-1.39	-2.35	-2.40	-2.77
	[-35.6]	[-27.1]	[-49.5]	[-15.1]	[-13.4]	
$AgInSe_2$	-1.71	-1.90	-1.26	-2.25	-2.22	–2.51
	[-31.8]	[-24.3]	[-49.5]	[-10.3]	[-11.4]	

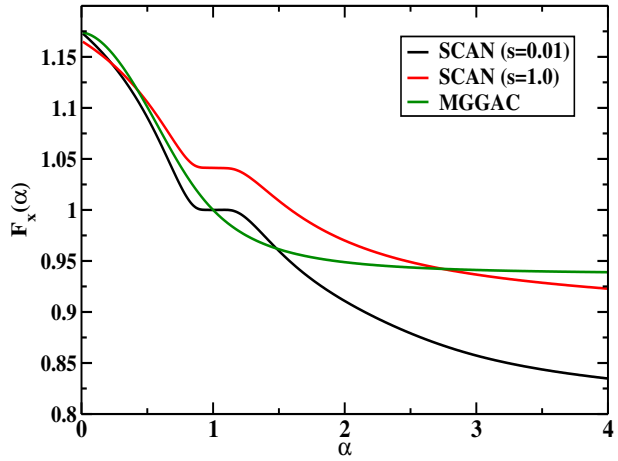

FIG. 8. The exchange enhancement factor of SCAN and MGGAC as a function of α for different values of reduced density gradient s. The MGGAC exchange is independent of s.

VI. RELATION BETWEEN PERFORMANCE AND MATHEMATICAL FEATURES OF FUNCTIONALS

Next, we discuss the plausible reasons behind improvement in performance of MGGAC functional over GGA or SCAN methods. To analyze the results, let us consider the behavior of the exchange enhancement factor (F_x) of SCAN and MGGAC functionals, the gKS potential of the meta-GGA functionals, and its relation to the derivative discontinuity (Δ_x), which is connected with the localized d- or f -states, often encountered in the chalcopyrite systems. In Fig. 8, we plot the F_x as a function of meta-GGA ingredient α for different values of reduced density gradient s. The MGGAC F_x does not depend on s and is much smoother than that for SCAN and its slope $\partial F_x/\partial\alpha$ is more negative in the energetically relevant regions of solids ($0 < s \leq 1$) resulting in inclusion of more $\Delta_x(\propto \partial F_x/\partial\alpha)$. In fact the negative slope $\partial F_x/\partial\alpha < 0$ is also connected to the ultranonlocality effect which results in polarization effect in solids[58]. Furthermore, the α is also interpreted as the measure of the well-known electron localization factor via the exchange energy, similar to the EXX[58]. Importantly, because of the more enhanced α dependent and $\partial F_x/\partial\alpha < 0$, some amount of inherent on-site Coulomb interaction (U) is included in the orbital energies and eigenvalues corresponding to MGGAC functional. The on-site Coulomb interaction (U) is important to treat the highly delocalized band states of rare-earth elements and strongly localized late transition metal elements. It may be noted that the SCAN functional also includes some amount of inherent U[77] which results in improved performances as compared to PBE+U and SCAN-no-U[78–82]. However, because of the more realistic and enhanced $\partial F_x/\partial\alpha < 0$, the MGGAC is a slightly better in treating the d- and f- orbitals and its results for chalcopyrite systems are often close to the HSE06, where the 25% HF exact exchange is used to treat the strongly localized d- bands. It may be noted that along with the localized d- states, the s- and p-states are also well described by the MGGAC. From the structure of the DOS plot (see Fig 6 and Fig. S3 of supporting information[65]) obtained using the MGGAC functional, one can readily observe that it treats the non-bonded Cu$-3d$ and hybridized $3d-4p$ (of Cu and Se) states in a bit better way than PBE and SCAN functionals. This results in the reduction of strong localization effect of $3d$ states, which in turn opens a sizable bandgap between occupied and unoccupied sub-bands.

In general, the success and overall improvement of MGGAC functional vis-a-vis LDA, GGA, and SCAN functioanls are retained for other chalcopyrite systems discussed in this article.

VII. CONCLUDING REMARKS

The comparative assessment of the structural properties, electronic properties, and formation energies of Cu-based multinary semiconductors is performed using GGA, meta-GGA, and hybrid density functionals within the framework of density functional theory. In particular, we assess the performances of SCAN, TM, and MGGAC meta-GGA functionals, which are very recent and reasonably successful exchange-correlation (XC) functionals in predicting various solid-state properties. To assess the structural properties, the tetragonal distortion (η) and/or anion displacement (u) are first computed from different functionals. The PBE-GGA functional is found to be inadequate to estimate accurately the electronic structures and associated properties of Cu-based chalcopyrite systems due to its inability to describe the intrinsic localization and/or strong correlation of the d electrons.

Our results for PBE and HSE06 are in agreement with earlier reported studies, wherein it was shown that the HSE06 generally improves over PBE because of less delocalization error, which in turn improves the bandgap, and density of state (DOS) estimates.

The estimates of various quantities computed using MGGAC and SCAN are found to be significantly improved as compared to those obtained using GGA. Further, the performances of MGGAC is found to be encouraging among meta-GGA functionals and quite close to that of the HSE06 in providing the estimates of η, u, band structures, and enthalpy formation energies of Cu-based multinary semiconductors. The reasonably improved and better performance of MGGAC is attributed to its a better description of strongly localized d electrons in these systems.

In addition, the performance of the aforementioned functionals is also explored for several competing candidate binary phases of Cu-Se. For these phases also, the MGGAC is found to be quite accurate. However, the SCAN functional performs slightly better than MGGAC for binary phases. The performance of TM functional is found to be poor in comparison to other meta-GGA functionals possibly due to its order of limit problem. Overall, our results strongly suggest that MGGAC (meta-GGA) functional can be highly useful for studying Cu-based multinary semiconductors as well as other systems with d-electrons, due to its good performance and low computational cost.

VIII. ACKNOWLEDGEMETS

A.G. would like to thank INSPIRE fellowship, DST, India for financial support. S.J. would like to thank NISER, Bhubaneswar for partial financial support. Calculations are performed high performance computing (HPC) clusters of IITH, Hyderabad. Part of calculations are also performed in the KALINGA and NISERDFT high performance computing (HPC) clusters of NISER, Bhubaneswar.

* ph17resch11006@iith.ac.in
† subrata.jana@niser.ac.in, subrata.niser@gmail.com
‡ manish@phy.iith.ac.in

[1] M. A. Green, Y. Hishikawa, E. D. Dunlop, D. H. Levi, J. Hohl-Ebinger, M. Yoshita, and A. W. Ho-Baillie, Progress in Photovoltaics: Research and Applications **27**, 3 (2019), https://onlinelibrary.wiley.com/doi/pdf/10.1002/pip.3102, URL https://onlinelibrary.wiley.com/doi/abs/10.1002/pip.3102.

[2] P. Jackson, D. Hariskos, E. Lotter, S. Paetel, R. Wuerz, R. Menner, W. Wischmann, and M. Powalla, Progress in Photovoltaics: Research and Applications **19**, 894 (2011), https://onlinelibrary.wiley.com/doi/pdf/10.1002/pip.1078, URL https://onlinelibrary.wiley.com/doi/abs/10.1002/pip.1078.

[3] A. Walsh, S. Chen, S.-H. Wei, and X.-G. Gong, Advanced Energy Materials **2**, 400 (2012).

[4] W. Feng, D. Xiao, J. Ding, and Y. Yao, Phys. Rev. Lett. **106**, 016402 (2011).

[5] J. C. Rife, R. N. Dexter, P. M. Bridenbaugh, and B. W. Veal, Phys. Rev. B **16**, 4491 (1977), URL https://link.aps.org/doi/10.1103/PhysRevB.16.4491.

[6] M. I. Alonso, K. Wakita, J. Pascual, M. Garriga, and N. Yamamoto, Phys. Rev. B **63**, 075203 (2001), URL https://link.aps.org/doi/10.1103/PhysRevB.63.075203.

[7] R. W. Birkmire and E. Eser, Annual Review of Materials Science **27**, 625 (1997), https://doi.org/10.1146/annurev.matsci.27.1.625, URL https://doi.org/10.1146/annurev.matsci.27.1.625.

[8] I. Repins, M. A. Contreras, B. Egaas, C. DeHart, J. Scharf, C. L. Perkins, B. To, and R. Noufi, Progress in Photovoltaics: Research and Applications **16**, 235 (2008), https://onlinelibrary.wiley.com/doi/pdf/10.1002/pip.822, URL https://onlinelibrary.wiley.com/doi/abs/10.1002/pip.822.

[9] M. A. Green, K. Emery, Y. Hishikawa, W. Warta, and E. D. Dunlop, Progress in Photovoltaics: Research and Applications **20**, 606 (2012), https://onlinelibrary.wiley.com/doi/pdf/10.1002/pip.2267, URL https://onlinelibrary.wiley.com/doi/abs/10.1002/pip.2267.

[10] S. N. Rashkeev and W. R. L. Lambrecht, Phys. Rev. B **63**, 165212 (2001), URL https://link.aps.org/doi/10.1103/PhysRevB.63.165212.

[11] H. W. Spiess, U. Haeberlen, G. Brandt, A. Räuber, and J. Schneider, physica status solidi (b) **62**, 183 (1974).

[12] J. Parkes, R. D. Tomlinson, and M. J. Hampshire, Journal of Applied Crystallography **6**, 414 (1973).

[13] J. J. Dittmer, E. A. Marseglia, and R. H. Friend, Advanced Materials **12**, 1270 (2000).

[14] J. Vidal, S. Botti, P. Olsson, J.-F. m. c. Guillemoles, and L. Reining, Phys. Rev. Lett. **104**, 056401 (2010).

[15] S. Siebentritt, M. Igalson, C. Persson, and S. Lany, Progress in Photovoltaics: Research and Applications **18**, 390 (2010), https://onlinelibrary.wiley.com/doi/pdf/10.1002/pip.936, URL https://onlinelibrary.wiley.com/doi/abs/10.1002/pip.936.

[16] W. Kohn and L. J. Sham, Phys. Rev. **140**, A1133 (1965).

[17] J. P. Perdew and Y. Wang, Phys. Rev. B **45**, 13244 (1992).

[18] J. P. Perdew, K. Burke, and Y. Wang, Phys. Rev. B **54**, 16533 (1996).

[19] A. J. Cohen, P. Mori-Sánchez, and W. Yang, Science **321**, 792 (2008), ISSN 0036-8075, https://science.sciencemag.org/content/321/5890/792.full.pdf, URL https://science.sciencemag.org/content/321/5890/792.

[20] F. D. Jiang and J. Y. Feng, Semiconductor Science and Technology **23**, 025001 (2007).

[21] J. Heyd, G. E. Scuseria, and M. Ernzerhof, J. Chem. Phys. **118**, 8207 (2003).

[22] J. Heyd and G. E. Scuseria, The Journal of Chemical Physics **121**, 1187 (2004), https://doi.org/10.1063/1.1760074, URL https://doi.org/10.1063/1.1760074.

[23] A. V. Krukau, O. A. Vydrov, A. F. Izmaylov, and G. E. Scuseria, J. Chem. Phys. **125**, 224106 (2006).

[24] J. Paier, M. Marsman, K. Hummer, G. Kresse, I. C. Gerber, and J. G. Ángyán, The Journal of Chemical Physics **124**, 154709 (2006).

[25] S. Jana, A. Patra, and P. Samal, J. Chem. Phys. **149**, 094105 (2018).

[26] S. Jana and P. Samal, Phys. Chem. Chem. Phys. **21**, 3002 (2019), URL http://dx.doi.org/10.1039/C8CP06715E.

[27] S. Jana, A. Patra, L. A. Constantin, and P. Samal, The Journal of Chemical Physics **152**, 044111 (2020), https://doi.org/10.1063/1.5131530, URL https://doi.org/10.1063/1.5131530.

[28] S. Jana, B. Patra, S. Śmiga, L. A. Constantin, and P. Samal, Phys. Rev. B **102**, 155107 (2020), URL https://link.aps.org/doi/10.1103/PhysRevB.102.155107.

[29] V. I. Anisimov and O. Gunnarsson, Phys. Rev. B **43**, 7570 (1991).

[30] V. I. Anisimov, F. Aryasetiawan, and A. I. Lichtenstein, Journal of Physics: Condensed Matter **9**, 767 (1997), URL https://doi.org/10.1088/0953-8984/9/4/002.

[31] V. I. Anisimov, J. Zaanen, and O. K. Andersen, Phys. Rev. B **44**, 943 (1991), URL https://link.aps.org/doi/10.1103/PhysRevB.44.943.

[32] Y. Zhang, X. Yuan, X. Sun, B.-C. Shih, P. Zhang, and W. Zhang, Phys. Rev. B **84**, 075127 (2011), URL https://link.aps.org/doi/10.1103/PhysRevB.84.075127.

[33] J. Sun, A. Ruzsinszky, and J. P. Perdew, Phys. Rev. Lett. **115**, 036402 (2015).

[34] J. Tao and Y. Mo, Phys. Rev. Lett. **117**, 073001 (2016).

[35] B. Patra, S. Jana, L. A. Constantin, and P. Samal, Phys. Rev. B **100**, 155140 (2019), URL https://link.aps.org/doi/10.1103/PhysRevB.100.155140.

[36] B. Patra, S. Jana, L. A. Constantin, and P. Samal, Phys. Rev. B **100**, 045147 (2019).

[37] A. Patra, S. Jana, and P. Samal, The Journal of Chemical Physics **153**, 184112 (2020), https://doi.org/10.1063/5.0025173, URL https://doi.org/10.1063/5.0025173.

[38] J. W. Furness, A. D. Kaplan, J. Ning, J. P. Perdew, and J. Sun, The Journal of Physical Chemistry Letters **11**, 8208 (2020).

[39] S. Jana, K. Sharma, and P. Samal, The Journal of Physical Chemistry A **123**, 6356 (2019).

[40] S. Jana, A. Patra, and P. Samal, J. Chem. Phys. **149**, 044120 (2018).

[41] S. Jana, K. Sharma, and P. Samal, J. Chem. Phys. **149**, 164703 (2018).

[42] Y. Zhang, J. Furness, R. Zhang, Z. Wang, A. Zunger, and J. Sun, Phys. Rev. B **102**, 045112 (2020), URL https://link.aps.org/doi/10.1103/PhysRevB.102.045112.

[43] Y. Zhang, C. Lane, J. W. Furness, B. Barbiellini, J. P. Perdew, R. S. Markiewicz, A. Bansil, and J. Sun, Proceedings of the National Academy of Sciences **117**, 68 (2020), ISSN 0027-8424, https://www.pnas.org/content/117/1/68.full.pdf, URL https://www.pnas.org/content/117/1/68.

[44] J. Nokelainen, C. Lane, R. S. Markiewicz, B. Barbiellini, A. Pulkkinen, B. Singh, J. Sun, K. Pussi, and A. Bansil, Phys. Rev. B **101**, 214523 (2020), URL https://link.aps.org/doi/10.1103/PhysRevB.101.214523.

[45] B. Patra, S. Jana, L. A. Constantin, and P. Samal, The Journal of Physical Chemistry C **125**, 4284 (2021), https://doi.org/10.1021/acs.jpcc.0c11380, URL https://doi.org/10.1021/acs.jpcc.0c11380.

[46] A. Patra, B. Patra, L. A. Constantin, and P. Samal, Phys. Rev. B **102**, 045135 (2020), URL https://link.aps.org/doi/10.1103/PhysRevB.102.045135.

[47] J. P. Perdew and K. Schmidt, in AIP Conference Proceedings (IOP INSTITUTE OF PHYSICS PUBLISHING LTD, 2001), pp. 1–20.

[48] G. Kresse and J. Hafner, Phys. Rev. B **47**, 558 (1993).

[49] G. Kresse and J. Furthmüller, Phys. Rev. B **54**, 11169 (1996).

[50] G. Kresse and D. Joubert, Phys. Rev. B **59**, 1758 (1999).

[51] G. Kresse and J. Furthmüller, Comput. Mater. Sci. **6**, 15 (1996), ISSN 0927-0256.

[52] P. E. Blöchl, Phys. Rev. B **50**, 17953 (1994).

[53] J. P. Perdew, W. Yang, K. Burke, Z. Yang, E. K. U. Gross, M. Scheffler, G. E. Scuseria, T. M. Henderson, I. Y. Zhang, A. Ruzsinszky, et al., Proc. Natl. Acad. Sci. U. S. A. **114**, 2801 (2017).

[54] Z.-h. Yang, H. Peng, J. Sun, and J. P. Perdew, Phys. Rev. B **93**, 205205 (2016).

[55] J. Sun, B. Xiao, Y. Fang, R. Haunschild, P. Hao, A. Ruzsinszky, G. I. Csonka, G. E. Scuseria, and J. P. Perdew, Physical review letters **111**, 106401 (2013).

[56] F. Della Sala, E. Fabiano, and L. A. Constantin, Int. J. Quantum Chem. **22**, 1641 (2016).

[57] J. P. Perdew, A. Ruzsinszky, J. Sun, and K. Burke, J. Chem. Phys. **140**, 18A533 (2014).

[58] T. Aschebrock and S. Kümmel, Phys. Rev. Research **1**, 033082 (2019), URL https://link.aps.org/doi/10.1103/PhysRevResearch.1.033082.

[59] Y. Mo, R. Car, V. N. Staroverov, G. E. Scuseria, and J. Tao, Phys. Rev. B **95**, 035118 (2017).

[60] Y. Mo, G. Tian, and J. Tao, Phys. Chem. Chem. Phys. **19**, 21707 (2017), URL http://dx.doi.org/10.1039/C6CP08761B.

[61] S. Jana, A. Patra, S. Śmiga, L. A. Constantin, and P. Samal, The Journal of Chemical Physics **153**, 214116 (2020), https://doi.org/10.1063/5.0028821, URL https://doi.org/10.1063/5.0028821.

[62] M. Lewin and E. H. Lieb, Physical Review A **91**, 022507 (2015).

[63] D. V. Feinblum, J. Kenison, and K. Burke, The Journal of Chemical Physics **141**, 241105 (2014), URL https://doi.org/10.1063/1.4904448.

[64] L. A. Constantin, A. Terentjevs, F. Della Sala, and E. Fabiano, Phys. Rev. B **91**, 041120 (2015).

[65] A. Ghosh, S. Jana, S. K. Behera, M. K. Niranjan, P. Samal, and L. A. Constantin, supporting information (2021).

[66] J. E. Jaffe and A. Zunger, Phys. Rev. B **28**, 5822 (1983).

[67] V. L. Shaposhnikov, A. V. Krivosheeva, V. E. Borisenko, J.-L. Lazzari, and F. A. d'Avitaya, Phys. Rev. B **85**, 205201 (2012).

[68] J. P. Perdew, A. Ruzsinszky, G. I. Csonka, O. A. Vydrov, G. E. Scuseria, L. A. Constantin, X. Zhou, and K. Burke, Phys. Rev. Lett. **100**, 136406 (2008).

[69] A. V. Terentjev, L. A. Constantin, and J. M. Pitarke, Phys. Rev. B **98**, 214108 (2018).

[70] N. Kim, P. P. n. Martin, A. A. Rockett, and E. Ertekin, Phys. Rev. B **93**, 165202 (2016), URL https://link.aps.org/doi/10.1103/PhysRevB.93.165202.

[71] H. Xiao, J. Tahir-Kheli, and W. A. Goddard, The Journal of Physical Chemistry Letters **2**, 212 (2011).

[72] A. Braga, S. Giménez, I. Concina, A. Vomiero, and I. Mora-Seró, The Journal of Physical Chemistry Letters **2**, 454 (2011), https://doi.org/10.1021/jz2000112, URL https://doi.org/10.1021/jz2000112.

[73] L. I. Berger, S. Bondar, V. V. Lebedev, A. D. Molodyk, and S. S. Strelchenko, Chemical Bond in Semiconductor and Semimetal Crystals (Nauka, Minsk, p. 248, 1973).

[74] V. Stevanović, S. Lany, X. Zhang, and A. Zunger, Phys. Rev. B **85**, 115104 (2012), URL https://link.aps.org/doi/10.1103/PhysRevB.85.115104.

[75] A. Jain, G. Hautier, S. P. Ong, C. J. Moore, C. C. Fischer, K. A. Persson, and G. Ceder, Phys. Rev. B **84**, 045115 (2011), URL https://link.aps.org/doi/10.1103/PhysRevB.84.045115.

[76] G. Hautier, S. P. Ong, A. Jain, C. J. Moore, and G. Ceder, Phys. Rev. B **85**, 155208 (2012), URL https://link.aps.org/doi/10.1103/PhysRevB.85.155208.

[77] H. Peng and J. P. Perdew, Phys. Rev. B **96**, 100101 (2017), URL https://link.aps.org/doi/10.1103/PhysRevB.96.100101.

[78] G. Sai Gautam and E. A. Carter, Phys. Rev. Materials **2**, 095401 (2018), URL https://link.aps.org/doi/10.1103/PhysRevMaterials.2.095401.

[79] J. Varignon, M. Bibes, and A. Zunger, Phys. Rev. B **100**, 035119 (2019), URL https://link.aps.org/doi/10.1103/PhysRevB.100.035119.

[80] N. E. Kirchner-Hall, W. Zhao, Y. Xiong, I. Timrov, and I. Dabo (2021), 2102.04636.

[81] R. B. Wexler, G. S. Gautam, and E. A. Carter, Phys. Rev. B **102**, 054101 (2020), URL https://link.aps.org/doi/10.1103/PhysRevB.102.054101.

[82] O. Y. Long, G. Sai Gautam, and E. A. Carter, Phys. Rev. Materials **4**, 045401 (2020), URL https://link.aps.org/doi/10.1103/PhysRevMaterials.4.045401.